Available online at www.sciencedirect.com
ScienceDirect
Journal of Catalysis 244 (2006) 199–207
JOURNAL OF CATALYSIS
www.elsevier.com/locate/jcat

Reaction rates of all hydrogenation steps in ammonia synthesis over a Ru(0001) surface

Christofer S. Tautermann, Yvette K. Sturdy, David C. Clary *

Physical and Theoretical Chemistry Laboratory, University of Oxford, South Parks Road, Oxford OX1 3HQ, United Kingdom

Received 27 September 2005; revised 23 August 2006; accepted 29 August 2006

Available online 11 October 2006

Abstract

The hydrogenation reactions of nitrogen ($NH_{n,(ads)} + H_{(ads)} \rightarrow NH_{n+1,(ads)}$, $n = 0, 1, 2$) on metal surfaces are important elementary steps in the catalytic formation of ammonia. We investigate the reaction dynamics of these hydrogenations on a Ru(0001) surface using transition state theory, including small curvature tunneling corrections. Potential energy surfaces are derived by density functional theory (RPBE) in two or three dimensions. Tunneling is shown to enhance rates significantly for the first two hydrogenation steps at low and ambient temperatures, doubling reaction rates even at temperatures of 400 K. However, tunneling plays no significant role at current synthesis temperatures.

Keywords: Ammonia catalysis; Hydrogenations; Tunneling; Surface reaction; Ruthenium; Reaction space Hamiltonian

1. Introduction

The Haber–Bosch process, in which ammonia is formed directly from gaseous hydrogen and nitrogen over a transition metal catalyst, has been used for approximately 100 years [1,2]. The most widely used catalyst for this process, iron, has the drawback of high operating pressures and temperatures [3,4]; therefore, other alternatives have been investigated [5]. Ruthenium has proven to be a very promising candidate [6–10], showing activity even at room temperature and atmospheric pressure [11].

Ammonia synthesis on ruthenium is, in analogy to that on iron [3,12], a multistep reaction, where the dissociative adsorption of nitrogen and hydrogen forms the first step. The adsorbed atomic species gather to form consecutively NH, NH_2, and finally NH_3, which desorbs from the surface in the last step. Zhang et al. [13] pointed out that a comprehensive understanding of the kinetics of the overall process can be gained only if rate constants for every single step in the catalytic cycle are derived. These can then be used to refine microkinetic models [14].

Because the dissociative adsorption of nitrogen on the metal surface is considered the rate-determining step, it has been investigated very well by experimental [15,16] and theoretical methods [13,17–22] and rate constants have been computed [21,23]. The effect of tunneling on the reaction rate is shown to be negligible if one considers the reactions on a stepped surface [23]. On a terrace, the barrier for reaction is much higher [21], and tunneling is proposed to be important [24]. The effect of the surface geometry on the dissociation barrier is huge, as the barrier drops from 1.9 to 0.4 eV when moving from a flat to a stepped surface [21]. Therefore, the dissociation reaction of N_2 on terraces may be neglected when modeling a real-world catalyst.

In contrast, there are just a few studies on the reaction rate constants of the hydrogenation steps [21,25,26], and the barriers are shown to be relatively unaffected on going from a flat to a stepped surface [21]. It has been shown that quite large tunneling effects must be considered [25,26], and at lower temperatures, the hydrogenation steps may become rate-determining [21]. Reaction rate constants that include tunneling are available for the first hydrogenation step ($N + H \rightarrow NH$), but estimates for the subsequent steps have not yet been calculated.

* Corresponding author.
E-mail addresses: christofer.tautermann@chem.ox.ac.uk (C.S. Tautermann), yvette.sturdy@chem.ox.ac.uk (Y.K. Sturdy), david.clary@chem.ox.ac.uk (D.C. Clary).

0021-9517/$ – see front matter
doi:10.1016/j.jcat.2006.08.023

The following hydrogenation steps are involved in ammonia synthesis:

$$N_{(ads)} + H_{(ads)} \rightleftharpoons NH_{(ads)}, \quad (1)$$

$$NH_{(ads)} + H_{(ads)} \rightleftharpoons NH_{2,(ads)}, \quad (2)$$

$$NH_{2,(ads)} + H_{(ads)} \rightleftharpoons NH_{3,(ads)}. \quad (3)$$

In the present study, we evaluate the tunneling effects and the reaction rate constants for all hydrogenation reactions (as well as the backward rate constants), to get a global picture of the whole hydrogenation process. The first two hydrogenation steps, (1) and (2), reveal quite significant enhancement by tunneling at moderate temperatures, whereas the last step, (3), is hardly influenced by tunneling due to heavy atom movement during the reaction.

2. Methods

2.1. DFT setup

The wave function is expanded in a plane wave basis with kinetic energy up to 25 Rydberg. A RPBE description of exchange and correlation effects [27] and ultrasoft pseudopotentials [28] are used. Self-consistent electron density is obtained by iterative diagonalization of the Kohn–Sham Hamiltonian. A supercell approach is applied to model the periodic geometry of the Ru(0001) surface. We choose a periodic array of (2×3) atoms with 2 layers as the unit cell, keeping the metal atoms fixed during all optimizations. Geometry optimizations are performed using quasi-Newton methods, and stationary points are confirmed by normal mode analysis with numerical second derivatives. The minimum energy paths (MEPs) are determined by a nudged elastic band (NEB) calculation [29], and refinement of the transition state is done using quasi-Newton steps.

The slab model is constructed by cleaving the (0001) face from the bulk Ru crystal with a geometry previously optimized with the same functionals. This or a very similar setup has already successfully been used in other studies describing ammonia catalysis on Ru(0001) [13,19,21,22,25,30]. All calculations are performed using the Dacapo program, developed by the Center for Atomic-Scale Materials Physics, DTU, Copenhagen [27,31] (available at: http://www.camp.dtu.dk/).

2.2. Definition of coordinates and computation of potential energy surfaces

To calculate tunneling contributions, we develop two- or three-dimensional potential energy surfaces (PESs) for all elementary steps (1)–(3).

2.2.1. $N_{(ads)} + H_{(ads)} \rightleftharpoons NH_{(ads)}$

Some recent studies have dealt with reaction rate constants and tunneling effects for this hydrogenation step [25,26,32]. These studies use fundamentally different PESs that are either generated for a different reaction mechanism with constraints [25] or derived on a model cluster using hybrid DFT [26].

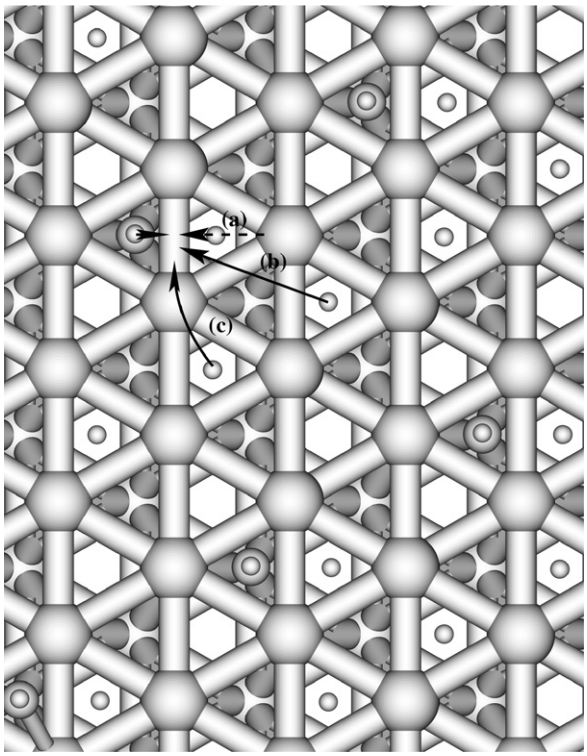

Fig. 1. Three different NEB-paths for the reaction of H with NH employing a $2 \times 3 \times 2$ unit cell.

There are some good reasons to use a PES derived by the supercell approach. First, it removes the worries about boundary effects; second, the supercell approach was previously applied to all hydrogenation reactions of nitrogen on ruthenium, always giving reliable and reasonable results. If we wished to proceed with the investigation with hybrid DFT on model clusters, then we would need to find an appropriate model cluster for all three reactions, which is currently unfeasible.

We take coordinates, the PES, rate constants, and tunneling contributions from a previous study [32] and present them here in the context of the other hydrogenation steps. We briefly review the coordinate definitions for completeness. During the reaction, hydrogen moves from an fcc site to a position on top of the nitrogen atom, which remains in an hcp site throughout the reaction. The hydrogen atom is confined to a plane orthogonal to the Ru(0001) surface, which includes the coadsorbed H and N species. To develop the PES, the hydrogen atom position is set to a total of 54 grid points in this plane, and the nitrogen atom is allowed to relax.

2.2.2. $NH_{(ads)} + H_{(ads)} \rightleftharpoons NH_{2,(ads)}$

The hydrogenation of NH to NH_2 is a more complex reaction, because it also includes movement of nitrogen from a threefold hollow hcp to a bridged site. The reacting hydrogen atom no longer moves in a plane, but rather takes a twisted path from the fcc site to the nitrogen. Various possible and obvious fcc starting points of the reacting hydrogen for the given NH coverage have been taken into account and are shown in Fig. 1. To get an impression of the coverage and possible impacts of the neighboring unit cells, more than one unit cell is shown.

Table 1
Relative energies in eV of the stationary points of various NEB-paths to form NH_2 or NH_3 on a Ru(0001) surface. The adsorbed reaction products are chosen as energy-zero. The paths correspond to Figs. 1 and 2

Path		Transition state	
	NH + H		NH_2
(a)	0.035	1.394	0.00
(b)	−0.493	1.382	0.00
(c)	−0.477	0.872	0.00
	NH_2 + H		NH_3
(d)	0.237	1.610	0.00
(e)	0.065	1.423	0.00
(f)	0.041	1.550	0.00

The starting geometry of path (a) (i.e., the hydrogen sits in a directly adjacent fcc site to NH) is not found to be an energy minimum.

Hydrogen does not stay at the fcc site, but moves closely to an on top site (starting point of the dashed arrow). For paths (b) and (c), the fcc sites constitute minima of the potential energy. Reaction profiles for all 3 paths are generated by the NEB-method [29]. The relative energies of the stationary points of the various paths are shown in Table 1. From these values, it is fairly obvious that we choose path (c) as a representative reaction path because the energy barrier is lower than for the other reaction paths. Although the energy of the coadsorbed NH + H species of path (b) is 0.4 kcal/mol lower than of path (c), the large difference in the barrier makes us confident that path (c) describes the reaction in the best way. If the coadsorbed geometry from path (b) is brought to reaction, then the mobile and light H atom is assumed to diffuse on the surface closer to NH first and then react via path (c).

According to this picture, we define a 3-dimensional Cartesian grid for the reacting hydrogen atom for reaction path (c). One axis is defined as the straight-line connection between the two ends of the MEP. The second axis is taken orthogonal to the first axis and is parallel to the Ru surface, while the third axis is obviously orthogonal to the two others. Altogether, hydrogen is kept fixed at 252 grid points, and the NH entity is allowed to relax. At each grid point, the constrained optimization is carried out using a quasi-Newton algorithm. There is also a small movement of nitrogen involved in the reaction; therefore, the choice of a 3-dimensional Cartesian Hamiltonian with the reduced mass of hydrogen must be made with care. Careful investigation will show that the imaginary frequency on the 3-dimensional PES is slightly larger than the imaginary frequency found by a full-dimensional transition state search. Therefore, scaling of the reduced mass of the coordinates is proposed and its effect on tunneling contributions discussed.

2.2.3. $NH_{2,(ads)} + H_{(ads)} \rightleftharpoons NH_{3,(ads)}$

The final hydrogenation step introduces significant flexibility into the system as the NH_2 entity moves from a bridged site to a position on top of a ruthenium atom, where it reacts with the hydrogen atom. Again, various reaction paths are investigated to choose a representative one for further calculations. Fig. 2 sketches 3 different paths on the surface, including some

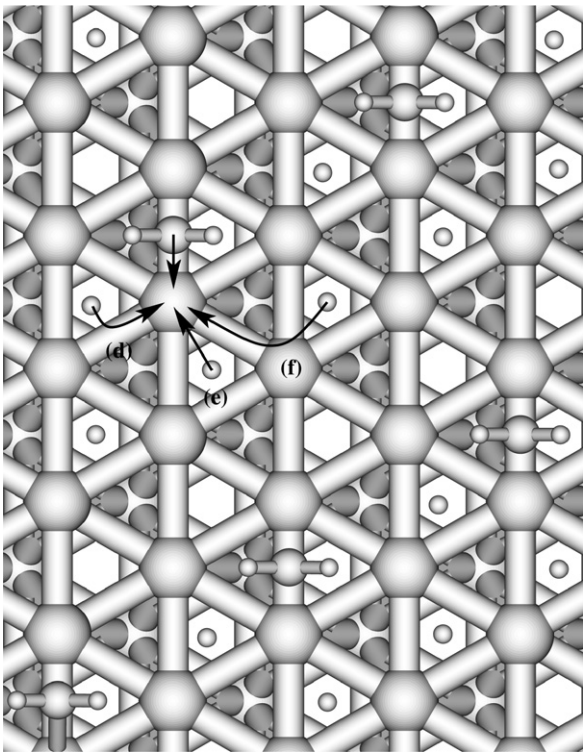

Fig. 2. Three different NEB-paths for the reaction of H with NH_2 employing a $2 \times 3 \times 2$ unit cell.

neighboring unit cells. In this case we choose path (e) to be representative for the reaction. The lowest energy of the coadsorbed states is found for path (f), which is about 0.6 kcal/mol lower than the reactants of path (e). But the barrier is found to be higher, and the reaction path is significantly longer than path (e). Path (d) has a similar barrier to path (e), but the energy of the coadsorbed H + NH_2 species is significantly higher (4 kcal/mol), making this reactant state less populated and this reaction less important.

All three NEB paths show a similar mechanism. The NH_2 entity moves toward the on top site to react with hydrogen rather than waiting at the bridged site for the approaching hydrogen. At the transition state, the NH_2 entity is close to the on top site, before the hydrogen atom begins to move significantly. This suggests two things: (1) Quantum effects will not be prominent in this reaction, because a substantial part of the reaction includes heavy atom movement, and (2) the PES cannot be derived as in the first two hydrogenation reactions, by simply moving the reacting hydrogen atom along a grid and relaxing the other atoms. This technique cannot work because the hydrogen stays close to the fcc site along a substantial part of the reaction path. The hydrogen atom moves most when the NH_2 entity is close to the top of the ruthenium atom, so only this part of the reaction path can be described by putting H on grid points and optimizing the NH_2 geometry.

For the reasons mentioned above, we take a different approach to the last hydrogenation reaction, which we call the "reaction space Hamiltonian" method. It is essentially a modification of the studies by Ruf and Miller [33] and Giese and Kühn [34], who define a very useful reaction plane Hamiltonian

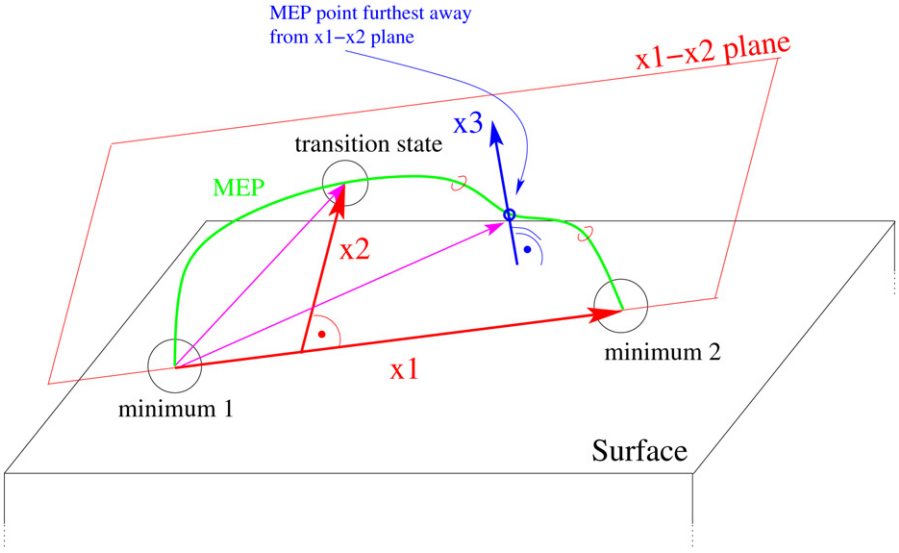

Fig. 3. The construction of axis directions for a reduced dimensionality PES.

in Cartesian coordinates based on the definition of the reaction plane of Yagi et al. [35]. We extend the approach from two to higher dimensions (hence the term "reaction space") and explain the advantages for surface reactions.

When deriving a reduced-dimensionality PES for dynamic calculations, one must be sure that the full-dimensional transition state and the full-dimensional minima (i.e., reactant and product geometries) are included to ensure that the reaction barriers are represented correctly. One way to define the first two axes is to span a plane that includes the minima and the transition state. Fig. 3 shows the axis definitions more clearly. Assuming that the adsorbed system consists of n atoms, the plane spanned by the $3n$-dimensional vectors $\overrightarrow{\min 2} - \overrightarrow{\min 1}$ and $\overrightarrow{\mathrm{TS}} - \overrightarrow{\min 1}$ contains the three stationary points ($\overrightarrow{\min 1}$ represents the reactant minimum, $\overrightarrow{\min 2}$ the product minimum, and $\overrightarrow{\mathrm{TS}}$ the coordinates of the transition state). All vectors are mass-weighted Cartesian position vectors relative to an arbitrary Cartesian coordinate system defined with respect to the metal surface. The axis directions x_1 and x_2 can be gained by orthogonalization of the two vectors (see Fig. 3). If one chooses to include more dimensions in the PES, there are different sensible ways to proceed. From a chemical standpoint, one approach is to include the largest fraction of the full-dimensional MEP possible in the PES. The MEP is a curved line in the $3n$-dimensional space and generally needs up to a $3n$-dimensional PES for it to be included completely. The definition of the first two coordinates guarantees inclusion of the parts of the full-dimensional MEP very close to the stationary points. The next coordinate may be chosen to include even more of the full-dimensional MEP in the PES. For this, it is convenient to identify a point along the MEP that is "furthest away" from the $x_1 - x_2$ plane. Thus, the definition of the distance of the MEP to the PES is a crucial point in the whole analysis. We choose the distance to be the Euclidean distance in the mass weighted set of coordinates. One could also weight the distance with the energy of the points on the MEP to get the high-energy regions described. Once the point on the MEP is chosen (we call it $\overrightarrow{\mathrm{pMEP}}$), the vector $\overrightarrow{\mathrm{pMEP}} - \overrightarrow{\min 1}$ together with the axis directions x_1 and x_2 spans a 3-dimensional PES, which includes all stationary points and a large fraction of the MEP. Orthogonalization gives the axis direction x_3 (see Fig. 3). One could proceed with this construction for more axis directions, but then the derivation of the grid for the PES would become unfeasible. Theoretically, one could continue until the full $3n$-dimensional Cartesian coordinate system is recovered. This method of defining the axis directions is accurate for catalytic reactions on surfaces, because the slab is much heavier than the adsorbates. The dimensionality of an n-atom adsorbate on a surface is $3n$ rather than $3n - 6(5)$ as it would be in gas phase due to translations and rotations. With a full $3n$-dimensional Cartesian coordinate system anchored in the slab, all aforementioned axis definitions are unique, and thus the Hamiltonian is simple:

$$\hat{H} = -\frac{\hbar^2}{2m_1}\frac{\partial^2}{\partial x_1^2} - \frac{\hbar^2}{2m_2}\frac{\partial^2}{\partial x_2^2} - \frac{\hbar^2}{2m_3}\frac{\partial^2}{\partial x_3^2} + V(x_1, x_2, x_3), \quad (4)$$

where m_1, m_2, and m_3 are the reduced masses along the coordinate directions. There are no mixing terms in the Hamiltonian, which makes it useful for application in various dynamical methods. Derivation of the potential $V(x_1, x_2, x_3)$ of Eq. (4) must be mentioned as well. In the optimal case, the system is kept fixed at various grid points in the (x_1, x_2, x_3) directions, and the other $3n - 3$ degrees of freedom are allowed to relax. This requires a constrained optimization at every grid point, where the directions of the three axes are projected out [36].

In our case, we use a total of 525 grid points in the space spanned by the x_1, x_2, and x_3 axes, where we calculate single energy points. Optimization of the geometry and inclusion of the zero-point energy (ZPE) at every grid point would be desirable, but is not feasible with the current computing power. Not optimizing and omitting the ZPE correction will introduce small errors, but this is still a first step estimating the tunneling contribution for the $NH_{2,(ads)} + H_{(ads)} \rightleftharpoons NH_{3,(ads)}$ step, and some refinement may be done in the future.

2.3. Transition state theory including tunneling

To evaluate reaction rate constants, we apply transition state theory, including quantum chemical effects such as tunneling and corner-cutting [37–44] to our system. TST rates are derived by the standard formula

$$k(T) = \kappa(T)\frac{k_B T}{h}\frac{Q^{\ddagger}(T)}{Q^{\min}(T)}\exp\left(-\frac{\Delta V^{\ddagger}}{k_B T}\right), \quad (5)$$

where the Q are the partition functions. $\Delta V^{\ddagger}$ is the zero point-corrected energy barrier for the reaction, and $\kappa(T)$ is the transmission coefficient, which accounts for tunneling, corner-cutting, and other nonclassical effects. Tunneling is taken into account by the small curvature tunneling (SCT) approach [42,45,46] in the framework of the semiclassical theory [47], which is expected to be a reliable technique for including tunneling corrections over a wide temperature range [48]. The SCT method assumes that the tunneling path is similar to the one suggested by Marcus and Coltrin [49], which follows the concave side classical turning points of the vibrations in the reaction valley. Specifically, we use the small-curvature semiclassical adiabatic ground state (SCSAG) approach [42], which determines tunneling for the adiabatic ground state of the system and includes nonclassical reflection on the barrier. The reaction path calculation is performed by the Page–McIver method [50], which uses first and second derivatives of the energy with respect to the coordinates. The step size is set to 0.01 a.u., and 200 (500 for reaction (3)) steps are taken in each direction, starting at the transition state. Reaction path information is stored as required for the SCT calculation.

Table 2
Structural parameters of all reactants, products and transition states. All distances are in Å. TS($NH_{n-1} \rightarrow NH_n$) corresponds to the transition state of reaction (n). For the transition states the imaginary frequencies from normal mode analysis are given

Species	Site or imag. frequency	Adsorption height	N–H bond length
H	fcc	1.08	–
N	hcp	1.20	–
NH	hcp	1.30	1.03
NH_2	bridge	1.67	1.03
NH_3	on-top	2.28	1.02
TS(N → NH)	1075i cm^{-1}	1.27	1.56
TS(NH → NH_2)	1150i cm^{-1}	1.39	1.44
TS(NH_2 → NH_3)	944i cm^{-1}	2.09	1.67

3. Results and discussion

3.1. Stationary points

All stationary points used for calculating rate constants are optimized by a quasi-Newton method and verified by normal mode analysis. The geometries found correspond well to previously published experimental and theoretical works [13,16,21,51,52]; geometric parameters are given in Table 2.

Reaction barriers for the reactions under study are given in Table 3. Our results compare well with previously published results [13,21,25,26]. The slight discrepancies with other studies may be explained by the use of a slightly different setup. Zhang et al. [13] used a different DFT functional, and Logadóttir and Nørskov [21] used a smaller unit cell. In addition, Zhang et al. [19] pointed out that there are various different transition states for each reaction, all with similar energies. We choose the reaction mechanisms with the lowest barriers and short MEPs to obtain higher reaction rate constants, as we discussed in a previous report [26].

According to the electronic energy barriers, either reaction (2) or reaction (3) could be the slowest step of the three hydrogenations, but adding zero-point energy corrections clearly identifies the second hydrogenation step as the one with the highest barrier. In addition, at higher temperatures, the free energy barrier of the second step is still significantly higher than that of the other steps. Fig. 4 shows the relative energy diagram for the hydrogenations and the influence of the zero point energy and vibrational entropy on the barriers [53]. The zero-point energy correction also has a very strong effect on the decomposition barrier of NH_3, lowering it by 20%. The energy of reaction of the last step even changes sign when including the zero point energy, making the NH_3 decomposition to H and NH_2 exothermic. This is also seen in experiments in which the decomposition of ammonia occurs concurrently with thermal desorption above room temperature [54,55].

Most intermediates of the ammonia synthesis on Ru(0001) have been experimentally identified with their structure and/or absorption site resolved [16,51,56–59]. The only elusive intermediate so far is NH_2, which has only been identified once at low temperature during hydrazine decomposition on Ru(0001), without obtaining further structural information [60]. The reason why it cannot be observed during hydrogenation of nitrogen or dehydrogenation of ammonia can be explained by referring to the energy diagram in Fig. 4. NH_2 has a higher energy than NH + H, and the barrier for dehydrogenation of NH_2 is low compared with the other (de)hydrogenation barriers. Therefore,

Table 3
Energy barriers in kcal/mol for the various hydrogenation steps

	$N + H \rightleftharpoons NH$		$NH + H \rightleftharpoons NH_2$		$NH_2 + H \rightleftharpoons NH_3$	
	Forward	Backward	Forward	Backward	Forward	Backward
Elec. barrier	24.7	31.9	31.1	20.0	31.3	32.8
ΔG(0 K)	23.7	27.8	30.3	15.9	28.5	26.5
ΔG(700 K)	23.1	27.3	29.3	16.2	26.4	25.5
Comparison	28 [21], 26.0 [13], 29.2 [25]	27.0 [13]	30 [21], 29.5 [13]	16.4 [13]	32 [21], 27.7 [13]	29.3 [13]

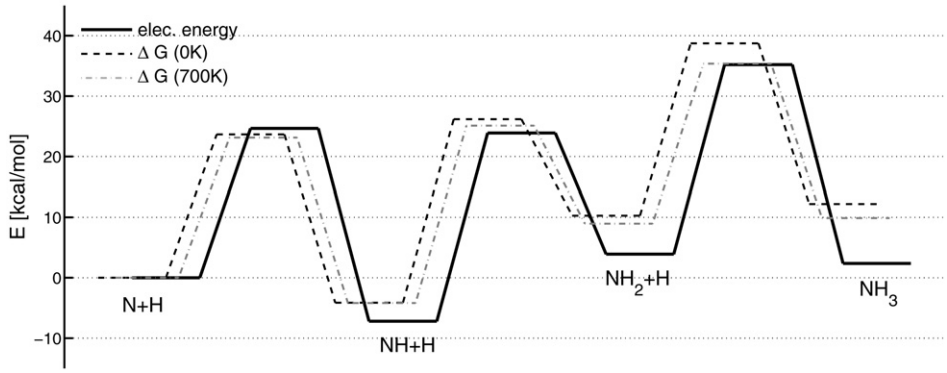

Fig. 4. Relative (free) energy diagram for the hydrogenation steps of nitrogen on Ru(0001).

the isolation of NH_2 on a surface is likely to be possible only at low temperatures, at which the species is kinetically stable. But from both sides (hydrogenation of nitrogen and dehydrogenation of ammonia), barriers of more than 25 kcal/mol must be overcome to yield NH_2. Thus, higher temperatures are required to get to the NH_2 intermediate, which is not stable at these temperatures. Thus, according to our calculated free energies, this intermediate will be present at a very low concentration during ammonia catalysis.

3.2. Potential energy surfaces and rate constants

The current study focuses on the reaction rate constants of the hydrogenation reactions of nitrogen to form ammonia on Ru(0001). One interesting question is whether one of these hydrogenation steps can become rate-determining at any temperatures relevant for catalysis. To answer this, a comparison to the N_2 dissociation step must be made. We use the TST rates for the N_2 dissociation on a stepped surface reported by Logadóttir and Nørskov [21] which we believe to be very reliable because van Harrevelt et al. [23] have shown that tunneling effects are negligible for this reaction. These two studies use the same electronic structure methods as the present study, making direct comparison of the rates both possible and useful. The rates of the hydrogenation steps are estimated from the rate constants in a similar way as was done by Logadóttir and Nørskov [21]. The difference in their study lies in the rate constants, which do not include semiclassical quantum tunneling contributions in contrast to the present study.

For all three PESs for reactions (1)–(3), the MEP is determined by the Page–McIver method [50], leading to the paths displayed in Fig. 5. The step size taken is rather small (0.01 au on the mass-scaled PESs), to ensure convergence of the paths and the tunneling corrections. The MEPs are all significantly curved, indicating the possibility of corner-cutting to shorten the tunneling path.

In the re-evaluation of the first hydrogenation step, tunneling was found to be less important than in a previous study [26]. This discrepancy can be easily explained by the use of different methods, as we used hybrid DFT on a model cluster in the other study. This leads to a narrower barrier and thus higher tunneling corrections. This methodological discrepancy has been discussed elsewhere [32], and for a useful comparison of all hydrogenation steps, all reactions should be treated by the same method.

The second hydrogenation step reveals a higher imaginary frequency at the transition state than the first (Table 2), so tunneling is expected to be more important. As mentioned in Section 2.2.2, the reaction also includes the movement of nitrogen, and therefore, the reduced mass along the three axis directions is presumably larger than the mass of hydrogen. A good measure of the correctness of the reduced masses is the imaginary frequency at the transition state (Table 2). If the reduced mass is too low, then the frequency on the 3-dimensional PES will be too high. Calculating the imaginary frequency on the 3-dimensional PES gives a value of $1333i\,\mathrm{cm}^{-1}$, which is slightly higher than the value in full dimensions. A possibility for taking the heavy atom movement into account is to scale the coordinate x_1, which corresponds to a reaction coordinate as it connects the two minima of the reaction, by the reduced mass of the transition vector. This will include the nitrogen movements in an implicit way, assuming that nitrogen moves homogeneously throughout the reaction. The mass scaling factor for the coordinate is 1.24, coming from a reduced mass of 1.54 of the transition vector. After mass scaling, the imaginary frequencies in full dimensions and on the 3-dimensional PES match.

For the third hydrogenation step, the imaginary frequency is lower, and tunneling does not play a significant role. Fig. 6 shows all transmission factors as a function of temperature, revealing that tunneling is most important in the second hydrogenation step. The enhancements by tunneling at room temperature come to 4.0, 10.2, and 1.6 for the reactions (1), (2), and (3), respectively. Because ruthenium also shows catalytic activity at these low temperatures [11], tunneling is definitely important for catalytic turnover. This picture clearly changes at the higher temperatures used for the industrial production of ammonia. At 700 K, the enhancement by tunneling is at most 30% for the hydrogenation reactions, nearly negligible.

To compare the calculated reaction rate constants to data in the literature and to understand the implications of the present findings, we calculate reaction rates in analogy to the study by Logadóttir and Nørskov [21]. These authors compared the TST rates of the hydrogenation steps on terrace sites to the rate-determining N_2 dissociation on step sites. Reaction rates for the

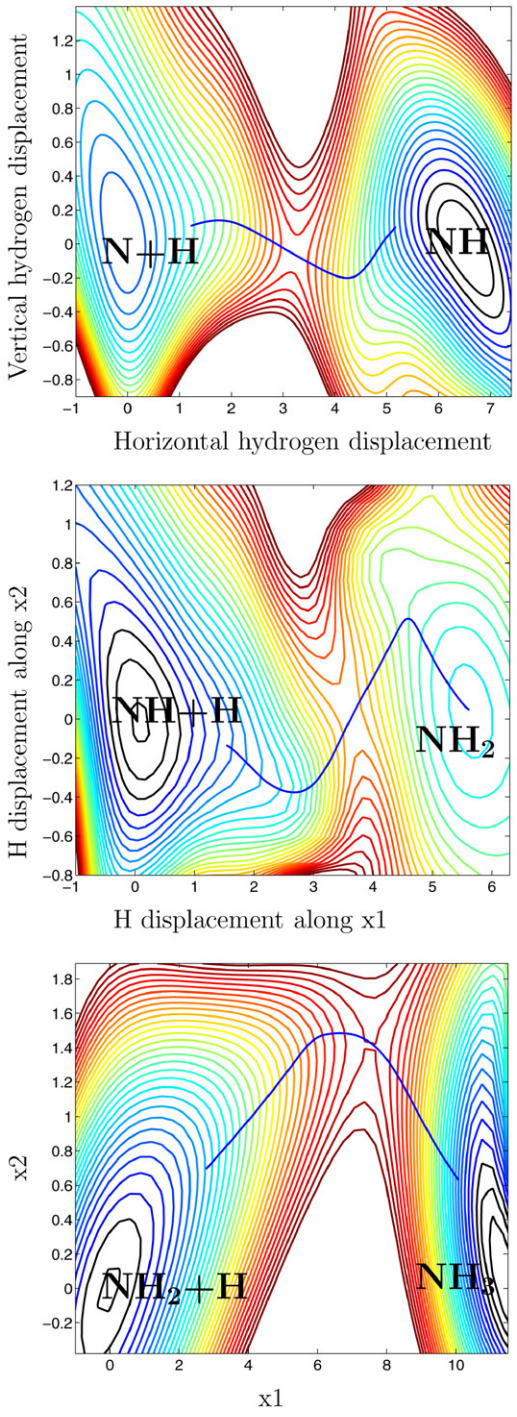

Fig. 5. Potential energy surfaces including minimum energy paths for reactions (1)—top, (2)—middle and (3)—bottom. For reactions (2) and (3) a cut through the MEP at the $x_3 = 0$ level is shown, as the PES is 3-dimensional. Coordinate axes are in atomic units and the coordinate definitions are given in the text.

N_2 dissociation are calculated by

$$r_N = k_N \frac{P_{N_2}}{P_0} \Theta_*^2, \tag{6}$$

where k_N is the rate constant for N_2-dissociation, P_{N_2} is the partial pressure of N_2, P_0 is the standard pressure (1 bar), and Θ_* is the number of free sites on the surface. Reaction rates for

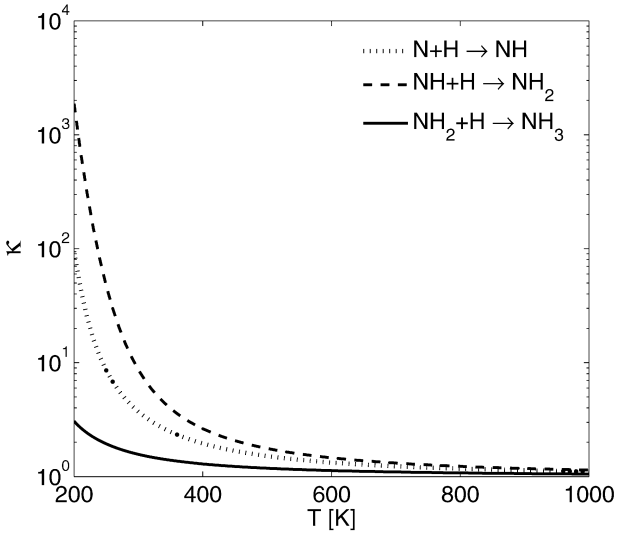

Fig. 6. Transmission probabilities by small curvature tunneling for the three hydrogenation steps in the ammonia synthesis over Ru(0001).

the hydrogenation steps are calculated by

$$r_{NH} = k_{NH} \Theta_N \Theta_H, \tag{7}$$

$$r_{NH_2} = k_{NH_2} \Theta_{NH} \Theta_H, \tag{8}$$

$$r_{NH_3} = k_{NH_3} \Theta_{NH_2} \Theta_H, \tag{9}$$

where k_{NH_x} are the rate constants for reactions (1)–(3). Θ_x stands for the surface coverage of species x. Under typical synthesis conditions, the number of free sites is rather low, and the surface coverage of intermediate products is generally assumed to be high [61].

Thus, we introduce the same approximation as Logadóttir and Nørskov [21] that just 1% of the Ru-surface consists of free sites and that the coverage of reaction intermediates is high. This also implies that there is no competition of the various hydrogenated species on the surface, which is quite a crude assumption, but thorough investigation of these interactions is beyond the scope of this study. The nature of this approximation does not influence our outcome that hydrogenation is faster than the N_2 dissociation, unless one considers conditions that are far from those used for ammonia synthesis.

Reaction rates for the hydrogenation steps are calculated and shown in Fig. 7. Our results confirm the outcome of Logadóttir and Nørskov that N_2 dissociation is the rate-determining step at temperatures relevant for catalysis. The crossover temperature of 320 K must not be taken as an absolute value for the crossover for ammonia synthesis, but rather as a qualitative number under the applied approximations. The inlay of Fig. 7 zooms into the region of the crossings of the rate, showing an interesting feature. Both the TST rate and the SCT rate of reaction (2) are displayed, indicating that tunneling enhancement shifts the crossover to approximately 15 K lower temperatures. This means that including tunneling in the rates predicts that N_2 dissociation is the rate-determining step over an even wider temperature range. Below room temperature, however, hydrogenation can become the rate-limiting step under the applied assumptions, where reactions (2) and (3) occur at almost the same

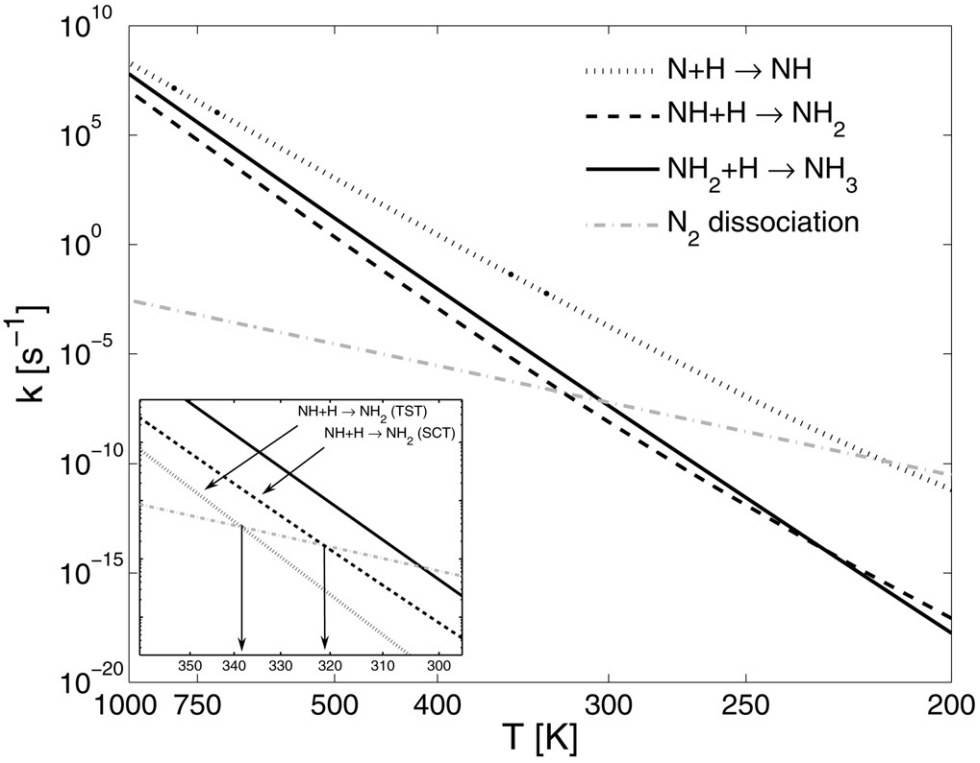

Fig. 7. Reaction rates of the stepwise hydrogenation reactions of nitrogen on Ru(0001) under the assumption of a high surface coverage and no interaction between different reactant-species. The magnified inlay compares the SCT-rate with the TST-rate of the second hydrogenation step and the rate for N_2 dissociation. Tunneling shifts the crossover for the change of the rate determining step to lower temperatures.

rate. At temperatures around 200 K, the rate of reaction (3) is predicted to be even lower than that of reaction (2), where it becomes the rate-determining step due to its lower tunneling contributions. However, the change in the rate-determining step at these low temperatures (200 K) is irrelevant for the catalytic mechanism, because the reaction rate at these temperatures is much too low for significant yields. We want to emphasize, however, that the reaction rates presented in this section are calculated for specific conditions (high coverage but no interaction of reaction intermediates). The accurate rate constants themselves (for the forward and backward reaction) are provided as supporting material.

4. Conclusion

Reaction rate constants, including tunneling corrections for the three hydrogenation steps of nitrogen to form ammonia (i.e., $N + H \rightarrow NH$, $NH + H \rightarrow NH_2$, $NH_2 + H \rightarrow NH_3$) on Ru(0001), and backward rate constants have been computed. Tunneling is taken into account by the small-curvature tunneling approach on 2- or 3-dimensional potential energy surfaces. Tunneling is important in the first two steps, where significant rate enhancement is predicted even at room temperature. But at the temperatures at which the industrial catalytic process is conducted (ca. 700 K), tunneling becomes negligible. Free energy profiles of the reaction steps help explain several experimental observations. The NH_2 entity is not observed during ammonia catalysis, because it cannot be kinetically stabilized at higher temperatures. Decomposition of ammonia occurs concurrently with desorption because the electronic barrier is significantly lowered by zero-point and entropic effects. This demonstrates that entropic effects are very prominent even in the hydrogenation of ammonia synthesis, and that they must be considered in models of the catalytic cycle.

Acknowledgments

C.S.T. acknowledges help from the Nørskov group (DTU, Copenhagen). Y.K.S. thanks the EPSRC for a doctoral studentship. Financial support was provided by the European Union Research Training Network grant HPRN-CT-2002-00170, “Predicting Catalysis: Understanding Ammonia Production From First Principles.”

Supporting material

Values of the reaction rate constants can be find at DOI: 10.1016/j.jcat.2006.08.023.

References

[1] F. Haber, G. van Oordt, Z. Anorg. Chem. 43 (1905) 111.
[2] K. Tamaru, in: J.R. Jennings (Ed.), Catalyic Ammonia Synthesis, Plenum Press, New York, 1991, pp. 1–18.
[3] A. Nielsen, An Investigation on Promoted Iron Catalysts for the Synthesis of Ammonia, 11th ed., J. Gjellerups Forlag, Copenhagen, 1956.
[4] K. Aika, in: A. Nielsen (Ed.), Ammonia: Catalysis and Manufacture, Springer-Verlag, Berlin, 1995, p. 103.

[5] S.R. Tennison, in: J.R. Jennings (Ed.), Catalyic Ammonia Synthesis, Plenum Press, New York, 1991, pp. 303–364.
[6] K.-I. Aika, H. Hori, A. Ozaki, J. Catal. 27 (1972) 424.
[7] S. Dahl, P.A. Taylor, E. Törnqvist, I. Chorkendorff, J. Catal. 178 (1998) 679.
[8] C.J.H. Jacobsen, S. Dahl, P.L. Hansen, E. Törnqvist, L. Jensen, H. Topsøe, D.V. Prip, P.B. Møenshaug, I. Chorkendorff, J. Mol. Catal. A 163 (2000) 19.
[9] D. Szmigiel, H. Bielawa, M. Kurtz, O. Hinrichsen, M. Muhler, W. Raróg, S. Jodzis, Z. Kowalczyk, L. Znak, J. Zieliński, J. Catal. 205 (2002) 205.
[10] S. Wu, J. Chen, X. Zheng, H. Zeng, C. Zheng, N. Guan, Chem. Commun. 19 (2003) 2488.
[11] K. Aika, Angew. Chem. Int. Ed. Engl. 25 (1986) 558.
[12] G. Ertl, in: J.R. Jennings (Ed.), Catalyic Ammonia Synthesis, Plenum Press, New York, 1991, pp. 109–132.
[13] C. Zhang, Z.-P. Liu, P. Hu, J. Chem. Phys. 115 (2001) 609.
[14] O. Hinrichsen, Catal. Today 53 (1999) 177.
[15] H. Dietrich, P. Geng, K. Jacobi, G. Ertl, J. Chem. Phys. 104 (1996) 375.
[16] S. Schwegmann, A.P. Seitsonen, H. Dietrich, H. Bludau, H. Over, K. Jacobi, G. Ertl, Chem. Phys. Lett. 264 (1997) 680.
[17] S. Dahl, Á. Logadóttir, R.C. Egeberg, J.H. Larsen, I. Chorkendorff, E. Törnqvist, J.K. Nørskov, Phys. Rev. Lett. 83 (1999) 1814.
[18] D.J. Dooling, R.J. Nielsen, L.J. Broadbelt, Chem. Eng. Sci. 54 (1999) 3399.
[19] C.J. Zhang, M. Lynch, P. Hu, Surf. Sci. 496 (2002) 221.
[20] Z. Cao, H. Wan, Q. Zhang, J. Chem. Phys. 119 (2003) 9178.
[21] Á. Logadóttir, J.K. Nørskov, J. Catal. 220 (2003) 273.
[22] K. Honkala, A. Hellman, I.N. Remediakis, Á. Logadóttir, A. Carlsson, S. Dahl, C.H. Christensen, J.K. Nørskov, Science 307 (2005) 555.
[23] R. van Harrevelt, K. Honkala, J.K. Nørskov, U. Manthe, J. Chem. Phys. 122 (2005) 234702.
[24] L. Romm, O. Citri, R. Kosloff, M. Asscher, J. Chem. Phys. 112 (2000) 8221.
[25] A. Volpi, D.C. Clary, J. Phys. Chem. B 108 (2004) 336.
[26] C.S. Tautermann, D.C. Clary, J. Chem. Phys. 122 (2005) 134702.
[27] B. Hammer, L.B. Hansen, J.K. Nørskov, Phys. Rev. B 59 (1999) 7413.
[28] D. Vanderbilt, Phys. Rev. B 41 (1990) 7892.
[29] G. Henkelman, H. Jonsson, J. Chem. Phys. 113 (2000) 9978.
[30] T.H. Rod, Á. Logadóttir, J.K. Nørskov, J. Chem. Phys. 112 (2000) 5343.
[31] S.R. Bahn, K.W. Jacobsen, Comput. Sci. Eng. 4 (2002) 56.
[32] C.S. Tautermann, D.C. Clary, Phys. Chem. Chem. Phys. 8 (2006) 1437.
[33] B.A. Ruf, W.H. Miller, J. Chem. Soc. Faraday Trans. 2 84 (1988) 1523.
[34] K. Giese, O. Kühn, J. Chem. Phys. 123 (2005) 054315.
[35] K. Yagi, T. Taketsugu, K. Hirao, J. Chem. Phys. 118 (2001) 10647.
[36] D.H. Lu, M. Zhao, D.G. Truhlar, J. Comput. Chem. 12 (1991) 376.
[37] H. Eyring, J. Chem. Phys. 3 (1935) 107.
[38] B.C. Garrett, D.G. Truhlar, J. Chem. Phys. 79 (1983) 4931.
[39] D.G. Truhlar, B.C. Garrett, Ann. Rev. Phys. Chem. 35 (1984) 159.
[40] B.C. Garrett, T. Joseph, T.N. Truong, D.G. Truhlar, Chem. Phys. 136 (1989) 271.
[41] A. Gonzalez-Lafont, T.N. Truong, D.G. Truhlar, J. Chem. Phys. 95 (1991) 8875.
[42] R.T. Skodje, D.G. Truhlar, B.C. Garrett, J. Phys. Chem. 85 (1981) 3019.
[43] D.G. Truhlar, A.D. Isaacson, B.C. Garrett, in: M. Baer (Ed.), Theory of Chemical Reaction Dynamics, CRC Press, Boca Raton, FL, 1985, pp. 65–137.
[44] S.C. Tucker, D.G. Truhlar, in: J. Bertran, I.G. Csizmadia (Eds.), New Theoretical Concepts for Understanding Organic Reactions, Kluwer Academic, Dortrecht, 1989, pp. 291–346.
[45] R.T. Skodje, D.G. Truhlar, J. Chem. Phys. 77 (1982) 5955.
[46] K.K. Baldridge, M.S. Gordon, R. Steckler, D.G. Truhlar, J. Phys. Chem. 93 (1989) 5107.
[47] M. Child, Semiclassical Mechanics with Molecular Applications, Clarendon Press, Oxford, 1991.
[48] C.S. Tautermann, B. Wellenzohn, D.C. Clary, Mol. Phys. 104 (2006) 151.
[49] R.A. Marcus, E. Coltrin, J. Chem. Phys. 67 (1977) 2609.
[50] M. Page, J.W. McIver, J. Chem. Phys. 88 (1988) 922.
[51] M. Staufer, K.M. Neyman, P. Jakob, V.A. Nasluzov, D. Menzel, N. Rösch, Surf. Sci. 369 (1996) 300.
[52] K.M. Neyman, M. Staufer, V.A. Nasluzov, N. Rösch, J. Mol. Catal. A 119 (1997) 245.
[53] D.A. McQuarrie, Statistical Thermodynamics, University Science Books, Mill Valley, CA, 1973.
[54] L.R. Danielson, M.J. Dresser, E.E. Donaldson, J.T. Dickinson, Surf. Sci. 71 (1978) 599.
[55] K. Jacobi, Y. Wang, C.Y. Fang, H. Dietrich, J. Chem. Phys. 115 (2001) 4306.
[56] C. Benndorf, T.E. Maddey, Surf. Sci. 135 (1983) 164.
[57] H. Shi, K. Jacobi, Surf. Sci. 313 (1994) 289.
[58] H. Shi, K. Jacobi, G. Ertl, J. Chem. Phys. 102 (1995) 1432.
[59] K.L. Kostov, W. Widdra, D. Menzel, Surf. Sci. 560 (2004) 130.
[60] H. Rauscher, K.L. Kostov, D. Menzel, Chem. Phys. 177 (1993) 473.
[61] S. Dahl, J. Sehested, C. Jacobsen, E. Törnqvist, I. Chorkendorff, J. Catal. 192 (2000) 391.